Functional characterization of the γ-aminobutyric acid transporter from *Mycobacterium smegmatis* MC^2 155 reveals sodium-driven GABA transport

Ana Pavić[a,b], Yurui Ji[a,c*], Agnese Serafini[d], Acely Garza-Garcia[d], Martin J. McPhillie[e], Alexandra O. M. Holmes[a], Luiz Pedro Sório de Carvalho[d], Yingying Wang[c], Mark Bartlam[f]#, Adrian Goldman[a,f,g]#, Vincent L. G. Postis[a,b]#.

[a]*Astbury Centre for Structural Molecular Biology, School of Biomedical Sciences, University of Leeds, Leeds, UK*

[b]*Biomedicine Research Group, Faculty of Health and Social Sciences, Leeds Beckett University, Leeds, UK*

[c]*College of Environmental Sciences & Engineering, Nankai University, Tianjin, China*

[d]*Mycobacterial Metabolism and Antibiotic Research Laboratory, The Francis Crick Institute, London, UK*

[e]*School of Chemistry, Faculty of Engineering & Physical Sciences, University of Leeds, Leeds, UK*

[f]*College of Life Sciences, Nankai University, Tianjin, China*

[g]*Molecular and Integrative Biosciences, University of Helsinki, Helsinki, Finland*

#Address correspondence to Adrian Goldman, A.Goldman@leeds.ac.uk, Vincent Postis, v.l.postis@leedsbeckett.ac.uk and Mark Bartlam, bartlam@nankai.edu.cn.

*Present address: New Energy Department, Tianjin Sino-German University of Applied Sciences, Tianjin, China.

Ana Pavić and Yurui Ji contributed equally to this work. Author order was determined on the basis of the length of the first names.

Running title: Sodium ions drive transport in *M. smegmatis* GabP

ABSTRACT

Characterizing the mycobacterial transporters involved in the uptake and/or catabolism of host-derived nutrients required by mycobacteria may identify novel drug targets against tuberculosis. Here, we identify and characterize a member of the amino acid-polyamine-organocation superfamily, a potential γ-aminobutyric acid transport protein, GabP, from *Mycobacterium smegmatis*. The protein was expressed to a level allowing its purification to homogeneity and Size Exclusion Chromatography-Multi Angle Laser Light Scattering analysis of the purified protein showed that it was dimeric. We showed that GabP transported γ-aminobutyric acid *in vitro* and when over-expressed in *E. coli.* Additionally, transport was greatly reduced in the presence of β-alanine, suggesting that it could be either substrate or inhibitor of GabP. Using GabP reconstituted into proteoliposomes, we demonstrated that γ-aminobutyric acid uptake is driven by the sodium gradient and is stimulated by membrane potential. Molecular docking showed that γ-aminobutyric acid binds MsGabP, another *Mycobacterium smegmatis* putative GabP and the *Mycobacterium tuberculosis* homologue in the same manner. This study represents the first expression, purification and characterization of an active γ-aminobutyric acid transport protein from mycobacteria.

IMPORTANCE

The spread of multidrug resistant tuberculosis increases its global health impact in humans. As there is transmission both to and from animals, the spread of the disease also increases its effects in a broad range of animal species. Identifying new mycobacterial transporters will enhance our understanding of mycobacterial physiology and furthermore provides new drug targets. Our target protein is the gene product of *msmeg_6196*, annotated as GABA permease, from *Mycobacterium smegmatis* strain MC^2 155. Our current study demonstrates that it is a sodium-dependent GABA transporter that may also transport β-alanine. As GABA may well be an essential nutrient for mycobacterial metabolism inside the host, this could be an attractive target for the development of new drugs against tuberculosis.

INTRODUCTION

Tuberculosis (TB), one of the oldest and deadliest human diseases, is caused by *Mycobacterium tuberculosis* (Mtb). Mtb is a leading infectious killer, claiming the lives of about 1.2 million people annually (1). It is a re-emerging pathogen, due to the development of multiple-drug resistant (MDR) and extensively-drug resistant (XDR) strains (2). In addition, animal tuberculosis is a globally distributed zoonotic chronic disease, posing a significant impact on the costs in global agricultural losses (3). Since transmission between humans and animals has been demonstrated in both directions, TB has been described as a One Health issue, having similar consequences for humans and animals (4), and causing huge socioeconomic impact both in terms of human lives and resources.

The unique cell wall composition of Mtb is believed to be the major determinant of its resistance to a large range of antibiotics (5), leading to a continuing need to discover new ones. A new approach to developing therapeutics against TB is through comprehensive discovery and characterization of metabolic pathways, their impact on key features of Mtb pathogenesis (6) and their contribution to drug resistance. Because Mtb has a reduced genome (7), it has neither extended *de novo* synthesis pathways nor duplicated transporters – the essential transmembrane proteins that mediate the nutrient uptake and metabolite efflux (8), meaning that there are many essential metabolites. The transporters, required for the uptake of essential nutrients, enable mycobacteria to persist in the harsh intracellular host environments by scavenging nutrients. They thus represent potential new drug targets. Characterizing unique mycobacterial transporters provides another route to discover novel therapeutics to treat TB (9).

Despite considerable progress in the development of genetic methods for mycobacteria the function of many transporters is still unknown. Nonetheless, AnsP1, an aspartate importer, was

identified by targeted mass-spectrometry based metabolomics. This method targets a pre-defined group of compounds and aims to determine which one is transported. A mixture of biomolecules is introduced into the mass spectrometer either directly or following a separation procedure. In particular, liquid chromatography-mass spectrometry-based targeted metabolomics achieves high level sensitivity and accuracy (10). AnsP1 was shown to be involved in nitrogen metabolism and essential for mycobacterial infection and survival (11-13). This provides evidence that Mtb relies on amino acid uptake and degradation pathways to thrive inside the host and confirms a strong link between nutrition and pathogenicity in Mtb.

To identify the substrates of other orphan transporters from mycobacteria, we adopted a similar approach for five homologous genes of AnsP1 from three different mycobacterial species. From this initial screen, the annotated GABA permease from *Mycobacterium smegmatis* MC^2 155, (MsGabP hereafter), proved promising for further studies. *M. smegmatis* is widely used as a convenient model system to study Mtb biology, cell structure and persistence under conditions of nutrient starvation (14) because it has a faster growth rate and lower biosafety level than *M. tuberculosis*. Based on its sequence, this putative permease belongs to the group of amino acid-polyamine-organocation (APC) superfamily of transport proteins (15), which is widely found in all living organisms. To date, no *in vivo* or *in vitro* information is available for *Mycobacterium smegmatis* GabP despite it being annotated as a probable GABA permease based on its sequence identity to *E. coli* GabP (16). The hydropathic profile produced by TMHMM2 predicted that MsGabP has twelve transmembrane-spanning helices (17). Homology modelling of the protein shows that it adopts an arrangement known as the LeuT fold (18) (Fig. S1).

In eukaryotes, besides its primary function as an inhibitory neurotransmitter (19), GABA may have a role in the modulation of immune responses (20) but it is unclear whether and how

GABAergic signalling regulates antimicrobial host defences during infections. GABA does, however, act as a specific cytotoxicity and virulence regulator of *Pseudomonas aeruginosa* (21). Bacteria, such as *Bacillus subtilis* (22), *P. syringae* (23) and isolated *E. coli* mutants (24), can use GABA as a sole nitrogen source. Furthermore, GABA is known to be important for acid resistance in bacteria including *E. coli* (25) and *Lactobacillus* (26). In the Mtb vaccine strain *M. bovis* BCG, uptake of GABA was not induced by carbon and nitrogen starvation (27). Beyond this, the mechanism and implications of GABA transport and metabolism have not been extensively examined in mycobacteria.

We report here the successful expression of *M. smegmatis* MC^2155 GabP in *E. coli.* SEC-MALLS analysis of the purified protein showed that it is a homodimer. *In vitro* and in live recombinant bacteria functional experiments allowed us to confirm predictions that it is a GABA transporter. We also showed that substrate uptake by MsGabP is sodium-driven and depends on the membrane potential.

RESULTS

MsGabP is expressed in *E. coli*.

MsGabP was inducibly expressed in *E. coli* under the control of the IPTG inducible promotor Tac. The expression level was tested by western blot in five strains and three different media (Fig. 1). In strains C41 (DE3) Δ*acrB* pRARE2 or C43 (DE3) Δ*acrB* pRARE2, we observed only a very low level of expression in SB medium (Fig. 1, panel 1S and 2S). Conversely, in the other strains, the expression level was higher when the cells were cultures in SB (Fig. 1, panel 3S, 4S and 5S) than in LB medium (Fig. 1, panel 3L, 4L and 5L). Densitometry measurements (Fig. S2) confirmed that MsGabP expresses best with BL21 Gold (DE3) pRARE2 as the strain in SB auto-induction medium. The expression level with C41 (DE3) Δ*acrB* and SB auto-induction medium was about 65% of that level (Fig. 1, panel 3S and 5S). We nonetheless chose this last condition for further optimization, since AcrB, which is a known contaminant of purified membrane protein from *E. coli*, is deleted in this last strain. Following further optimization (data not shown), we determined that the optimal expression conditions in C41 (DE3) Δ*acrB* strain was SB auto-induction medium for 24 hours at 37 °C.

The protein eluted at approximately 36 kDa on sodium dodecyl sulfate-polyacrylamide gel electrophoresis (SDS-PAGE), though the predicted molecular mass is 50.7 kDa. (see *Purification of MsGabP* below).

Targeted Metabolomics suggest GABA and serine as potential substrates of MsGabP.

We used targeted metabolomics to identify potential substrates (see *Materials and Methods*). We expressed MsGabP in *E. coli* using the pL33 plasmid and tested for uptake of following amino acids: GABA, arginine, lysine, aspartate, asparagine, glutamine, glutamate and serine.

142 The rationale was as follows: GABA because MsGabP is annotated as a GABA permease;
143 arginine and lysine because it belongs to the APC superfamily of transporters; aspartate,
144 asparagine, glutamine, glutamate because it has about 35-36% identity to Mtb AnsP1 and
145 AnsP2, which transport asparagine; and serine, which is polar but not charged, as a negative
146 control. We observed a two-fold differential in internal GABA concentration with 1 mM
147 GABA in energized *E. coli* cells containing MsGabP (Fig. 2A). Similarly, with 5 mM serine,
148 there was about a seven-fold differential (Fig. 2B), suggesting these two amino acids could
149 represent potential substrates. No transport of the other tested amino acids was detected. For
150 instance, neither 1 mM nor 5 mM arginine and aspartate increased the concentration of the
151 respective amino acid in the MsGabP cells compared to control cells (Fig. S3).

152

153 **MsGabP transports radiolabelled GABA into cells.**

154 To confirm the uptake of potential amino acids by MsGabP, we next performed radiolabelled
155 transport assays on intact cells. Consistent with the metabolomics study results, *E. coli* cells
156 overexpressing MsGabP are able to uptake radioactive GABA (Fig. 3). As control, cells (empty
157 plasmid) only showed a negligible uptake of radioactive GABA. This clearly shows that the
158 uptake of GABA was indeed due to the overexpressed MsGabP and not linked to *E. coli*
159 endogenous GABA transporters. In contrast, radioactive serine was not transported by
160 MsGabP, suggesting that serine is not a true substrate of the transporter (data not shown).
161 Interestingly, β-alanine, a structural analogue of GABA, competed with the uptake of
162 [^{3}H]GABA into energized *E. coli* whole cells (Fig. 3), suggesting that it might bind as a
163 competitive inhibitor of GABA. GABA uptake was also significantly decreased when a
164 protonophore, 50 μM of carbonylcyanide m-chlorophenylhydrazone (CCCP), was added with

GABA to the assay (Fig. 3), indicating that the transport depends on the proton gradient and/or on the membrane potential.

Purification of MsGabP.

We next wanted to study the transport of amino acids with purified and reconstituted MsGabP and we therefore tested a range of detergents for solubilization efficiency. n-Decyl-β-D-Maltopyranoside (DM), n-Undecyl-β-D-Maltopyranoside (UDM), n-Undecyl-β-D-Thiomaltopyranoside (UDTM) and n-Dodecyl-β-D-Maltoside (DDM) at 1% all extracted MsGabP from the membranes with similar efficiencies (~80%), as quantified after western blot analysis (Fig. 4A). Since DDM has a lower critical micellar concentration (CMC) than DM, we decided to proceed with DDM for solubilizing the protein in large scale purification.

Preliminary purifications in DDM showed that the purified protein was unstable and contained contaminants (not shown). We therefore used the HRV-3C-His-tag to perform on-column detergent exchange followed by on-column cleavage to elute MsGabP to identify detergents that stabilized the purified protein. To identify the best one, small scale purifications were conducted with 12 different detergents (Table 1). The stability was then assessed by microscale fluorescent thermal stability assay (28). The protein unfolded cooperatively in DDM, Decyl Maltose Neopentyl Glycol (DMNPG), UDTM, n-Dodecyl-β-D-Thiomaltopyranoside (DDTM) and n-Tridecyl-β-D-Maltopyranoside (13M) (Fig. 4B) under the buffer conditions tested. This suggests that MsGabP is correctly folded in all of these detergents. However, it was most stable in 13M or DMNPG (T_m of 51.4 ± 0.1°C and 51.2 ± 0.2°C) (Fig. 4B), which is about 4°C higher than in DDM (Fig. 4B). As the final yield from DMNPG was higher than from 13M (Table 1), we used DMNGP for further experiments. Yields of ~0.7 mg protein per litre of bacterial culture were typically achieved.

Fractions collected during the protein elution from the resin showed the presence of two bands, migrating at ~36 kDa and ~70kDa respectively (Fig. 5A). Peptides generated by tripsin digestion of the protein bands were analyzed using mass spectrometry. The acquired spectra were analyzed in PEAKS software, which allowed us to identify MsGabP with 12 unique peptides and a total sequence coverage of 14% in the lower band at 36 kDa and 2 unique peptides and a total sequence coverage of 3% in the upper band at 70 kDa (Fig. S4). In the lower 36 kDa band we are able to detect peptides from the N-terminus, the middle of the MsGabP and the C-terminus, consistent with a full-length protein, as is shown by the fact that it is active in GABA transport (see below). The 70 kDa band is either a protein homodimer or a partially folded monomer, but most likely the latter (29).

Purified MsGabP is a dimer.

The absolute molecular weight of the purified protein-detergent complex was determined by SEC-MALLS (Fig. 5B). The protein eluted as a single, symmetrical peak at ~0.4 column volume, demonstrating its homogeneity and mono-dispersion (Fig. 5B). Using the three-detector method (30), the molecular mass of MsGabP in the main peak was found to be 79.2 ± 5.7% kDa, indicating the protein is dimeric in the protein-detergent complex.

MsGabP-driven GABA transport depends on both Na^+ and membrane potential.

To study MsGabP function free from *E. coli* metabolism and interference by its endogenous amino-acid transporters, we reconstituted purified MsGabP into liposomes. The migration ('flotation') of proteoliposomes on a discontinuous sucrose gradient demonstrated successful reconstitution of the protein into liposomes with an efficiency of ~90% (Fig. S5), as a majority

of the proteoliposomes float into the 5% and 2.5% fractions of the gradient. We were therefore able to use these to study the transport mechanism of MsGabP.

Radioactive transport assays showed there was a significantly higher accumulation of ^{3}H-GABA in proteoliposomes containing MsGabP as compared to protein-free liposomes (MsGabP *vs* control), when proteoliposomes loaded with K^+ were diluted into a buffer with Na^+ (Fig. 6A). We were unable to measure any transport of ^{3}H-GABA into proteoliposomes using pH gradients alone (Fig. 6B/CCCP). In contrast, the addition of the potassium-conducting ionophore valinomycin (31) in the transport buffer (with Na^+ present) established a negative inside potential that led to increased GABA transport compared to the uptake level in the absence of valinomycin (Fig. 6B/Val). When the membrane potential generated by valinomycin is abolished by the addition of CCCP, the uptake activity was negligible (Fig. 6B/Val and CCCP). Importantly, when choline chloride was used in place of NaCl in the presence of valinomycin, GABA uptake was abolished completely indicating that Na^+ was essential for transport (Fig. 6B/Val, compare Na^+ out *vs* ChoCl out). To confirm that the pH gradient does not contribute to GABA transport, we trapped a membrane impermeant fluorescent pH indicator, pyranine, in the proteoliposomes. No change in pH was recorded in upon the addition of GABA in MsGabP containing proteoliposomes. This confirms that protons are not involved in GABA uptake (Fig. 6C).

Phylogenetic analysis shows that *E. coli* GabP and *B. subtilis* GabP are closely related to MsGabP and MtbGabP

A tblastn search against mycobacterial genomes using *E. coli* GabP and an E-value of e^{-100}, retrieved sequences across the whole span of *Mycobacteria*, including sequences from the pathogenic species *M. tuberculosis*, *M. ulcerans*, *M. avium* and *M. abscessus*. The primary

sequences of MsGabP and MtbGabP (Rv0522) are 47% identical (56% BLOSUM62 score similar), while MsGabP and *E. coli* GabP are 43% identical (62% similar). We also noted that the gene product of *msmeg_5473* (Ms5473 hereafter) shares 49% identity with MtbGabP and 41% identity with MsGabP, suggesting that it is also closely related to MtbGabP. A phylogenetic tree of bacterial protein sequences related to *E. coli*, *B. subtilis* and *M. tuberculosis* GabP shows there are two different groups of GabP sequences, each containing members from Proteobacteria, Bacilli and Actinobacteria. The first group includes the sequences from *E. coli* (P25527), *Pseudomonas syringae* (Q87UE3), *Bacillus subtilis* GabP (P46349), *Streptomyces coelicolor* (Q9L202) and *Corynebacterium glutamicum* AroP (Q46065), a protein characterised as an aromatic amino acid transporter. The second group has a less varied taxonomic distribution and comprises mainly Actinobacteria sequences, including MsGabP and MtbGabP, but also Bacillales, α– and β-Proteobacteria (Fig. S6).

Docking studies suggest that the residues involved in GABA binding are conserved between MsGabP, MtbGabP and Ms5473.

To identify potential substrate binding sites in the MsGabP, MtbGabP and Ms5473 models (see *Methods and Materials)*, molecular docking of GABA to the models with Grid-based Ligand Docking with Energetics (Glide) software (32) was performed. All predicted GABA binding poses exhibited clusters located in the same area of the protein (Fig. S7), corresponding to the outward-facing occluded conformation of the transporter as found in L-arginine/agmatine antiporter AdiC (33). The residues that interact with GABA are strongly conserved and form conserved interactions with the ligand, suggesting that they are involved in substrate binding, consistent with GABA binding to all three transporters. The side chain of E119 (in MsGabP)/E89 (in MtbGabP) appears to hydrogen bond to the γ-amino group in GABA, while

this interaction is absent in Ms5473. Instead, it appears to interact with S297, which would be a weaker interaction (Fig. S7).

DISCUSSION

The ability of Mtb to adapt its metabolism to environmental changes, including various stress conditions, is believed to be critical for its pathogenicity (34). It is known that amino acids support growth of Mtb *in vitro* (12). However, we lack knowledge about the regulation of amino acid transport and metabolism in mycobacteria. The identity of many transporters involved in this process in Mtb is still unknown.

Here we characterize, for the first time, the putative mycobacterial GABA permease from *M. smegmatis* strain MC^2 155. MsGabP is closely related to MtbGabP and *M. bovis* GabP (27) (47% sequence identity) and to the previously characterized GABA permeases from *B. subtilis* (35) and *E. coli* (24) (48% and 43% sequence identity) respectively. GABA transport is an important aspect of GABA metabolism and is regulated in concert with GABA catabolism enzymes in other bacteria. Although nitrogen-limited culture conditions induce GABA permease expression in *E. coli* and *B. subtilis* (36, 37) the regulatory mechanisms are different. As in *B. subtilis* (22) GabP and metabolic enzymes in mycobacteria are not physically clustered, suggesting it might exhibit functional characteristics distinct from the *E. coli* GabP, where there is coordinated regulation of the *gab* gene cluster (24, 38).

MsGabP was successfully expressed in C41 (DE3) Δ*acrB* cells grown in SB auto-induction (Fig. 1) medium with a yield of 0.7 mg/L culture, extending the success of using pTTQ18 based plasmids for the expression of a range of membrane transporters (39). This provided us with a platform for our metabolomics and other studies. We initially used *in vivo* (using a heterologous host) targeted metabolomics to identify potential MsGabP substrates. Our metabolomics analysis suggested that GABA and serine might both be substrates of MsGabP (Fig. 2), but not asparagine, aspartate or lysine (Fig. S3).

Further functional characterization, using radiolabelled uptake assays with energized *E. coli* whole cells (Fig. 3), clearly demonstrated MsGabP mediated GABA uptake, and therefore confirmed that MsGabP is a GABA transporter. Uptake rate was in the range of ~0.05 µmol/mg cells, but it was essentially abolished, to ~0.01 µmol/mg cells in the presence of 50 µM CCCP (Fig. 3). Similarly, CCCP inhibited GABA uptake by non-homologus GabP in *C. glutamicum* (40). We have shown however that GABA uptake does not involve protons, therefore suggesting that transport is dependent on membrane potential rather than proton gradient. GABA uptake by MsGabP was also sensitive (~70%) to competition with β-alanine (Fig. 3), as previously observed for both eukaryotic (41) and prokaryotic (42) GABA transporters. Unfortunately, we could not measure uptake of β-alanine as we could not obtain it radiolabelled. Therefore, we could not determine if β-alanine is only a competitor or if it is a true MsGabP substrate. Interestingly, *B. subtilis* GabP transports β-alanine 500 times more efficiently than the *E. coli* transporter, reflecting the differences in binding domains of various GABA permeases (42).

We next aimed to purify MsGabP, to perform more reliable transport measurements in proteoliposomes. We screened for conditions that maintain protein stability and monodispersity prior to reconstitution. Membrane protein purification strategy success depends on the type of detergent used for solubilization and the subsequent purification steps. The on-column detergent exchange method adopted here represents a fast, versatile and economical approach to screen a series of detergents (43–44). Solubilization trials (Fig. 4A) of membrane preparation from cells with amplified expression of MsGabP using 12 different detergents at a concentration of 1% identified DDM as the best detergent. Though DDM can extract MsGabP efficiently from the membrane, DMNPG was preferred for its ability to stabilize the protein and was therefore used in downstream experiments.

Purified MsGabP was found to be dimeric in DMNPG (Fig. 5). This is not uncommon amongst this family: mouse GAT1 appears to form both dimers and high-order oligomers as shown by *in vivo* FRET experiments (45). Li and colleagues (46) showed that Fos-Choline 12 purified GABA transporter from *E. coli* is monomeric in solution. The difference in oligomerisation state is probably due to the FC-12, which is zwitterionic and much harsher than DMNPG, and so presumably denatures the protein (47, 48).

We reconstituted MsGabP into proteoliposomes with 90% efficiency (Fig. S5). The presence of proteoliposomes in the upper fractions upon flotation on discontinuous sucrose gradient reflects successful protein incorporation (49). Like other secondary active transporters, substrate uptake by GABA transporter is driven by electrochemical ion gradients (50) and the co-transported ions vary among different organisms. Direct measurement of GABA transport with proteoliposomes showed that GABA uptake was tightly coupled with sodium cations (Na^+) (Fig. 6), as previously seen in a non-homologus *C. glutamicum* transporter (40).

A phylogenetic analysis (Fig. S6) of closely related sequences to GabP shows that this group of transporters is present across different classes of bacteria and includes the experimentally characterized GABA transporters of *E. coli*, *B. subtilis* and *P. syringae*, although at least one member, Ncgl1062 from *C. glutamicum*, has been shown to be an aromatic amino acid transporter. All *Mycobacterium* species analysed have one GabP sequence for which the phylogenetic distribution follows the evolutionary history of the genus, suggesting that it was present in the last common ancestor of all mycobacteria. It is reasonable to assume that in this orthologous cluster, the ability to transport GABA is preserved and that the annotation of Rv0522 as a GABA permease is appropriate. Some mycobacteria have a second GabP sequence that was probably acquired by lateral gene transfer, from within the same group of transporters: this includes *M. smegmatis*. Here we have shown that this second member is also a GABA transporter. Finally, structural analysis of the docked complexes revealed a similar

binding pocket for GABA in all three homologues, with GABA being recognized by conserved amino acids residues (Fig. S7). The poses for MsGabP and MtbGabP are more similar than that of Ms5473, supporting our argument that both MsGabP and MtbGabP are GABA transporters. We can only speculate, but MsGabP and Ms5473 may differ in when they are expressed, and/or in their relative affinities for GABA, as is the case in *S. aureus*, which has two proline transporters (51).

GABA may be an important metabolite required for mycobacterial pathogenesis, raising the therapeutic potential of inhibitors towards GABA permease. We hope these studies will lead to structural and further biochemical exploration of this novel mycobacterial transporter, resulting in the discovery of new potent drugs against TB.

MATERIALS AND METHODS.

General. The primers used for PCR were from Sigma-Aldrich (St. Louis, MO, USA), enzymes for cloning from New England Biolabs (Ipswich, MA, USA), the reagents for the bicinchoninic acid (BCA) assay from Thermo Fisher Scientific (Waltham, MA, USA), His tag horseradish peroxidase-conjugated antibody from Bio-Techne (Minneapolis, MN, USA), detergents from Anatrace (Maumee, OH, USA), and radiolabelled γ-[2,3-3H(N)]-aminobutyric acid ([^{3}H]GABA) from Perkin Elmer (Waltham, MA, USA). All other chemicals were from Sigma-Aldrich (St. Louis, MO, USA) and were of analytical grade or better. The *Mycobacterium smegmatis* MC^2 155 strain was purchased from ATCC (Manassas, VA, USA), C41 (DE3) Δ*acrB* from Lucigen Corporation (Middleton, WI, USA), BL21 Gold (DE3) from Stratagene (La Jolla, CA, USA), BL21 Star (DE3) from Thermo Fisher Scientific (Waltham, MA, USA) and plasmid pRARE2 from Novagen (the Merck Group, Darmstadt, DE). All media, buffers and other solutions were prepared using deionized water. All media were sterilized by autoclaving or for thermally sensitive solutions by passage through 0.2 μM filters from Millipore.

Cloning. An expression vector pL33 for the production of MsGabP was constructed by using the vector pTTQ18 (52). pL33 encodes a C-terminal His tag preceded by an HRV-3C protease cleavage site (53). The gene *msmeg_6196* encoding GabP was amplified with *M. smegmatis* MC^2 155 genomic DNA as template by PCR using the upstream primer with *Nhe*I site, *5'*-GCTAGCCTCGAATCGAGATCCGATCTG-*3'*, and downstream primer with *Sbf*I site *5*'-CCTGCAGGCTCATCGGTTCTCGCAGC-*3'*. The amplified fragment was digested with *Nhe*I and *Sbf*I and inserted between the corresponding sites of plasmid pL33 to construct the expression plasmid pL33-MsGabP.

Cell growth and membrane preparation. Expression tests for MsGabP were performed using *E. coli* strains: C41 (DE3) Δ*acrB*, C41 (DE3) Δ*acrB* pRARE2, C43 (DE3) Δ*acrB* pRARE2, BL21 Gold (DE3) pRARE2 and BL21 Star (DE3) pRARE2 and three different types of media for cell growth (Lysogeny broth (LB), Superbroth (SB) and M9 auto-induction media) in 24 deep-well plates (Whatman plc, GE Healthcare, IL, USA) at 37°C for 24 h with shaking at 1,300 rpm (54). Isopropyl β-D-1-thiogalactopyranoside (IPTG) induction and auto-induction were compared to determine which condition produced more of the target protein. 10 µg of lysed cells (54) was loaded onto SDS-PAGE and protein expression determined by western blot using His tag horseradish peroxidase-conjugated antibody. Large-scale expression of MsGabP was performed in a 30 L fermentor (Infors HT). The cells were grown in SB auto-induction medium at 37°C for 24 h and harvested by centrifugation (6000 x g, 20 min, 4°C). The cells were resuspended in 1 × PBS buffer (10 mM Na_2HPO_4, 1.8 mM KH_2PO_4, 137 mM NaCl, 4 mM KCl, pH 7.4) with a ratio of 6 ml buffer/g cells. Membranes were prepared following the protocol in (54), resuspended with 1 × PBS buffer and total protein concentration in the membrane was measured by BCA assay (55).

Solubilization and purification of MsGabP. The solubilization test was carried out at 4°C with 12 different detergents (Table 1). The membrane fraction of *E. coli*/MsGabP adjusted to 2 mg/ml was incubated in 20 mM Tris (pH 8.0), 150 mM NaCl, 10% (v/v) glycerol and 1% (w/v) of the tested detergent at 4°C for 1 h. Samples before and after centrifugation at 100,000 × g for 1 h were analyzed by western blot. Purification was started with 100 mg of total membrane protein that was homogenized and solubilized for 1 h at 4°C in solubilization buffer (10 mM Na_2HPO_4, 1.8 mM KH_2PO_4, 4 mM KCl, 287 mM NaCl, 7.5 mM imidazole, 10% (v/v) glycerol, pH 7.4) with 1% (w/v) DDM at a protein concentration of 5 mg/ml, followed by removal of insoluble material by centrifugation at 100,000 × g for 1 h. The supernatant was incubated with 1 ml HisPur™ cobalt resin (50% slurry) (Thermo Fisher

Scientific, Waltham, MA, USA), pre-equilibrated with wash buffer 1 (same composition as the solubilization buffer) containing 0.05% (w/v) DDM at 4°C, for 2 h with gentle mixing. Immobilized-metal affinity chromatography (IMAC) was performed by mixing the supernatant with the equilibrated resin for 2 h with gentle mixing. The resin was then packed into the Econo-Pac® disposable gravity-flow chromatography column (Bio-Rad, Hercules, CA, USA). Unbound material was collected followed by washing of the column with ~10 x column volumes of wash buffer 1 and 2 (differing from wash buffer 1 only by the imidazole concentration, which was 10 mM).

On-column detergent exchange. Detergent was exchanged on-column from DDM into CYMAL 6, β-OG, OGNPG, DMNPG, LMNPG, DM, UDM, UDTM, DDTM, 13M and 14M by replacing DDM in the wash buffer 2 with 3 × CMC of each detergent. The resin then was washed with a wash buffer 3 (20 mM HEPES, (pH 7.0), 100 mM NaCl, 5% (v/v) glycerol, 3 × CMC of detergent) for 8 x column volume to remove imidazole. HRV-3C protease was then added at a molar ratio of 1:1 to the target protein to the resin with a minimal volume of wash buffer 3 and incubated at 4°C overnight to cleave the His tag. The following day, the protein was eluted from the column using ~7 ml of a wash buffer 3 and then concentrated to a volume of ~100 µl by centrifugation using a concentrator with a MW cut off of 50 kDa (Vivaspin 2, Sartorius).

Microscale fluorescent thermal stability assay. The stability of the protein purified in different detergents was checked by microscale fluorescent thermal stability assay as described in (28) with the following modifications. The buffer used for dilution of the dye N-[4-(7-diethylamino-4-methyl-3-coumarinyl)phenyl] maleimide (CPM) was the same as the buffer that the protein sample was eluted with. After briefly mixing the dye and the protein sample, the mixture was equilibrated at room temperature for 10 min while protecting it from light, and

then placed into the Stratagene Mx3005P Real Time PCR machine (Agilent Technologies, Santa Clara, CA, USA). The ramp rate was 4°C/min and the starting and ending temperatures were 25°C and 90°C. Data were processed with GraphPad Prism program (GraphPadPrism for Mac, GraphPad Software, San Diego, CA, USA [http://www.graphpad.com/scientific-software/prism/]).

Size Exclusion Chromatography-Multi Angle Laser Light Scattering. The molecular mass and the oligomerization state of the purified MsGabP was determined via size exclusion chromatography coupled to light scattering, absorbance and differential refractive index detectors method. The refractive index and light scattering detectors were from Wyatt Technology (Goleta, CA, USA) and the UV detector and chromatography pumps from Shimadzu Corporation (Kyoto, Japan). The Superose 6 column (WTC-MP030S5 (Wyatt Technology, Goleta, CA, USA)) was equilibrated with 20 mM HEPES (pH 7.0), 100 Mm NaCl, 5% (v/v) glycerol, 0.0102% (w/v) DMNPG overnight. 30 µl of MsGabP (3 mg/ml) was injected and the sample eluted from the column was analyzed by three detectors (30). Data obtained were analyzed using ASTRA software package, version 6.1 (Wyatt Technology, Goleta, CA, USA). The program calculated $M_{W,protein}$, $M_{W,detergent}$ and $M_{W,total}$ throughout the peak and also provides information on the monodispersity of the peak (56).

Targeted metabolomics study. *E. coli* strain C41 (DE3) Δ*acrB* harbouring pL33 or pL33-MsGabP were cultured in 50 ml LB medium at 37°C for 8 h in 250 ml shaker flasks. 10^8 cells were transferred onto mixed cellulose filters (pore size: 0.22 µm, Merck Millipore, Billerica, MA, USA) by vacuum filtration and then incubated overnight at 30°C in agar plates (1.5% (w/v) containing minimal medium (50 mM Na_2HPO_4, 50 mM KH_2PO_4, 25 mM $(NH_4)_2SO_4$, 2 mM $MgSO_4$, trace metals, vitamins, 0.5% glucose) supplemented with ampicillin (100 µg ml^{-1}). The cells were adapted for 1 h at 37°C. Filters with the cells were transferred onto

minimal medium agar (1.5% (w/v)) plates supplemented with the specific amino acid tested (1 mM or 5 mM), 0.5 mM IPTG and ampicillin (100 μg ml^{-1}), and incubated for 0.5 h at 37°C. The cells were harvested and transferred to 1 ml acetonitrile/methanol/water (2:2:1 v/v/v) solution. The cells were then disrupted using a bead beater and polar metabolites were extracted. After centrifugation, supernatants were collected and filtered with 0.22 μm spin-X column filters (Costar, Corning Inc., NY, USA). Extracts were stored at -80°C before analysis. The amino acids tested were arginine, aspartate, asparagine, GABA, glutamate, glutamine, lysine, and serine. The liquid chromatography-mass spectrometry was performed as described (57). Aqueous normal phase liquid chromatography was performed using an Agilent 1200LC system with a flow rate of 0.4 ml/min. Elution of polar compounds was performed using a gradient of solvents A (Milli-Q water and 0.2% acetic acid) and B (acetonitrile and 0.2% acetic acid). Accurate mass spectrometry was performed using an Agilent Accurate Mass 6230 TOF apparatus equipped with Multi-mode Ion source. Data were analyzed using Qualitative Analysis B.07.00 software and the metabolites were identified comparing the accurate m/z (error less than 10 ppm) and the retention time with the accurate m/z and the retention time of standard solutions for the specific metabolite. The ions counts were recorded and normalized to the residual protein content (detected by BCA assay) present in each extract.

Whole-cell radiolabeled assay. C41 (DE3) Δ*acrB E. coli* was grown in M9 minimal medium supplemented with glycerol (20 mM) and carbenicillin (100 μg ml^{-1}) in volumes of 50 ml at 37°C in 250 ml baffled conical flasks with aeration at 200 rpm to an OD_{680} of ~0.4–0.6. The cells were then either un-induced or induced with IPTG (0.5 mM) for further 1 h. Harvested cells (by centrifugation at 2500 x g for 10 min) were washed three times with 40 ml of buffer (5 mM MES, pH 6.6, 100 mM NaCl and 50 mM KCl) and then resuspended to a cell density of A_{680} ~2.0. Cell suspension (196 μl) containing 20 mM glycerol was aerated in a bijou bottle held in a water jacket at 37°C for 3 min, and then [^{3}H]GABA (50 μM) with a specific activity

of 10 μCi/ml was added with brief mixing. Exactly 10 min after adding the [^{3}H]GABA, 80 μl aliquots were transferred to cellulose nitrate filters (0.45 μm pore size), pre-soaked in transport buffer, on a vacuum manifold and washed with transport buffer (6 ml). The filters were transferred to scintillation vials with 10ml Emulsifier-Safe liquid scintillation fluid (Perkin Elmer) and incubated overnight. The level of [^{3}H] radioactivity was measured by liquid scintillation counting (Packard Tri-Carb 2100TR instrument, Perkin Elmer, Waltham, MA, USA). The measured value of disintegrations per minute was converted into μmol/mg cells. Background counts were measured by washing filters under vacuum in the absence of cells or radiolabeled substrate. Standard counts were measured by transferring 1, 2.5, 5 and 10 μl radiolabeled substrate stock solution directly to a washed filter in the vial.

To test the effect of CCCP on transport, it was added at a final concentration of 50 μM. To test the effect on [^{3}H]GABA uptake, unlabelled β-alanine (final concentration 5 mM) was added to the cells prior to energizing the proteoliposomes. [^{3}H]GABA was added 5 min after and 80 μl aliquot was taken to measure the radioactivity.

Protein reconstitution and liposome flotation assay. The *E. coli* lipid extract (Avanti Polar Lipids, Inc.) dissolved in chloroform was dried under nitrogen and the lipid film was resuspended by vortexing to 10 mg/ml with reconstitution buffer (25 mM HEPES (pH 6.8), including 200 mM KCl and 1 mM DTT). The dissolved lipid was then passed eleven times through 0.4 μm and then 0.2 μm pore size filters (polycarbonate Nucleopore Track Etch membrane filters) placed inside the barrel of the extruder. To destabilize the liposomes and allow the insertion of the membrane protein, 1.1% β-octyl glucoside (OG) was added to 1 ml of liposomes. The purified protein was added at 500:1 lipid to protein ratio and incubated at 4°C for 1 hour. This was then diluted to 15 ml with a reconstitution buffer and centrifuged at 100,000 x g for 1 h at 4°C. Liposome pellets were resuspended in 1 ml of the reconstitution

buffer. Proteoliposomes were analyzed using a flotation assay in sucrose gradient made of layers containing 60%, 30%, 10%, 5% and 2.5% (mass/vol.) sucrose. 250 µl of proteoliposomes were added to 250 µl of 60% sucrose (in 1 x HEPES buffer, pH 6.8). This fraction was overlaid with 0.5 ml of 30% sucrose, 20%, 10%, 5% and finally 0.4 ml of 2.5% sucrose. After centrifugation at 259,000 x g for 16 h, the fractions were collected from the gradient, and analyzed for protein by SDS-PAGE.

Fluorimetric transport assay. The proteoliposomes (5 µL) loaded with 25 mM HEPES (pH 6.8) 200 mM KCl and 1mM pyranine dye were diluted in a buffer (1 mL) containing 25 mM HEPES (pH 6.8), 200 mM NaCl and equilibrated in a stirred cuvette in the Photon Technology International QM-1 spectrophotometer (PTI, U.K.) for 3 min. Fluorescence was monitored using 400 and 450 nm excitation and 509 nm emission. To induce membrane potential, valinomycin was added (5 nM) at ~60 sec, followed by the addition of 30 mM GABA at ~160 sec and 0.03 mM CCCP at ~200 sec. The internal pH change was monitored as a change in the ratio of 450:400 nm pyranine fluorescence (58).

Radiolabeled assay with proteoliposomes. GABA transport was initiated by diluting 6.6 µl of proteoliposomes loaded with 25 mM HEPES (pH 6.8) 200 mM KCl buffer into 330 µl of external transport buffer: either 25 mM HEPES (pH 6.8) 200 mM NaCl buffer or 25 mM HEPES (pH 6.8) 200 mM choline chloride. To determine whether the presence of membrane potential ($\Delta\Psi$) was needed to drive GABA uptake, 5 nM valinomycin and/or 0.03 mM CCCP were added to the transport buffers. The incubation time was about 60 seconds before starting the reactions by addition of [^{3}H]GABA (specific activity 10µCi/mL) at a final concentration of 50 µM. 10 min after adding the radiolabeled substrate, 80 µl aliquots were transferred to cellulose nitrate filters (0.45 µm pore size) pre-soaked in transport buffer on a vacuum manifold and washed immediately with transport buffer (6 ml). The filters were transferred to

scintillation vials and radioactivity measured as described for the whole cell assay. The measured value of disintegrations per minute was converted into pmol/mg protein/min.

Phylogenetic analysis. The sequences of Cluster of Orthologous Groups 1113 were downloaded from EggNOG (59) and clustered using an 80% identity threshold with CD-HIT (60). An alignment was calculated using Mafft v7.310 FFT-NS-2 (61). Sequences with less than 400 residues were removed and the alignment was simplified to less than 85% redundancy with Jalview 2.11 (62). Both termini were truncated to the first and the last column with 100% occupancy.

Independently, in-house scripts and BLAST+ (63) were used to mine mycobacterial and selected model bacteria sequences using the sequence of *E. coli* GABA permease as query and an expect threshold of e^{-100}. Matches were aligned with MUSCLE (64) and the alignment was truncated and simplified to less than 95% redundancy as previously explained. Both alignments were combined using Mafft and checked for redundancy and partial/truncated and very divergent entries were removed.

The cluster of GabP sequences was then extracted leaving behind those of related the transporters, *e.g*. AnsP (P9WQM7), CycA (O33203), YifK (P27837), ProY (P0AAE2), pheP (P24207), LysP (P25737) and yvbW (O32257). A final alignment of this cluster was calculated using Mafft G-INS-I and consisted of 273 sequences. The best-fit evolutionary model for the alignment was LG+F+R6 as calculated by ModelFinder (65). Maximum likelihood phylogenetic analysis was done using IQ-TREE v1.6.11 (66) with 100 standard bootstrap replicates. Phylogenetic trees were visualized with Dendroscope (67).

Molecular model of GabPs and molecular docking of GABA. *De novo* protein modelling of MsGabP was performed using the Robetta server (68). The protein structures of MtbGabP and Ms5473 were homology-modelled by Phyre2 (69), using MsGabP protein sequence as query. The rank matches for both models had 50% identity and 100% confidence, indicating high probability of modelling success. The graphical user interface Maestro (version 12.4, Schrodinger LLC, New York, NY, 2020) was used to visualise the three protein models, which were prepared for molecular modelling using the Protein Preparation Wizard (default settings). The GABA ligand was drawn in Maestro and a low energy, zwitterionic conformation was generated using Ligprep (version 12.4 Schrodinger LLC, New York, NY, 2020). A 36 Å receptor grid encompassing the protein structure was generated centred on a user-defined residue (MsGabP G223, MtbGabP T193, Ms5473 V210). Molecular docking of the GABA ligand was performed on each protein model using Glide in SP mode using default settings but outputting 15 poses (version 12.4, Schrodinger LLC, New York, NY, 2020). The predicted binding poses of the GABA ligand were ranked by docking score and the list visually inspected for predicted hydrogen bonding and their associated directionality and length, steric clashes/unfavourable interactions, and ligand conformations. A GABA binding pose within each protein model was chosen based on the above criteria.

ACKNOWLEDGEMENTS

The authors are grateful for financial support from the Leeds Beckett University (to A. P. and V. L. P.), China Scholarship Council (to Y. J.), the Wellcome Trust (ref.019322/7/10/Z), the Erkko Foundation and the BBSRC (BB/M021610/1) (to A. G.), and the Francis Crick Institute, which receives its core funding from Cancer Research UK (FC001060), the UK Medical Research Council (FC001060), and the Wellcome Trust (FC001060) (to L. P. C.), the Wellcome Trust (104785/B/14/Z) to L. P. C., the National Science Foundation of China (31870053 to M. B. and 31670498 to Y. W.). AG acknowledges his Royal Society Wolfson Research Merit Award**.** The authors thank Dr. Maren Thomsen for performing the SEC-MALLS analysis, Dr. Steven Harbone for providing suggestions on the microscale fluorescent thermal stability assay, Dr. James Ault for performing the Mass Spectrometry protein analysis, Lotta Happonen for help with the Mass Spectrometry analysis and Prof. Peter J. F. Henderson and David Sharples for use of the fermentation facilities at the Faculty of Biological Sciences, University of Leeds.

570 **REFERENCES**

571 1. 2020. WHO | Global tuberculosis report 2019.

572 2. Seung KJ, Keshavjee S, Rich ML. 2015. Multidrug-Resistant Tuberculosis and Extensively
573 Drug-Resistant Tuberculosis. Cold Spring Harb Perspect Med 5:a017863.

574 3. Teppawar RN, Chaudhari SP, Moon SL, Shinde SV, Khan WA, Patil AR. 2018. Zoonotic
575 Tuberculosis: A Concern and Strategies to Combat. Basic Biology and Applications of
576 Actinobacteria. IntechOpen.

577 4. Kaneene JB, Miller R, Steele JH, Thoen CO. 2014. Preventing and controlling zoonotic
578 tuberculosis: a One Health approach. Vet Ital 50:7–22.

579 5. Jarlier V, Nikaido H. 1994. Mycobacterial cell wall: Structure and role in natural resistance
580 to antibiotics. FEMS Microbiol Lett 123:11–18.

581 6. Rhee K. 2013. Minding the gaps: metabolomics mends functional genomics. EMBO Rep
582 14:949-950.

583 7. Stinear TP, Seemann T, Harrison PF, Jenkin GA, Davies JK, Johnson PDR, Abdellah Z,
584 Arrowsmith C, Chillingworth T, Churcher C, Clarke K, Cronin A, Davis P, Goodhead I,
585 Holroyd N, Jagels K, Lord A, Moule S, Mungall K, Norbertczak H, Quail MA,
586 Rabbinowitsch E, Walker D, White B, Whitehead S, Small PLC, Brosch R, Ramakrishnan
587 L, Fischbach MA, Parkhill J, Cole ST. 2008. Insights from the complete genome sequence
588 of *Mycobacterium marinum* on the evolution of *Mycobacterium tuberculosis*. Genome Res
589 18:729–741.

590 8. Lodish H, Berk A, Zipursky SL, Matsudaira P, Baltimore D, Darnell J. 2000. Overview of
591 membrane transport proteins, *In* Molecular cell biology, 4th ed, WH Freeman, New York.

592 9. Cook GM, Berney M, Gebhard S, Heinemann M, Cox RA, Danilchanka O, Niederweis M.
593 2009. Physiology of Mycobacteria. Adv Microb Physiol 55:81–182, 318–319.

594 10. Roberts LD, Souza AL, Gerszten RE, Clish CB. 2012. Targeted metabolomics. Curr Protoc
595 Mol Biol Chapter 30:Unit 30.2-30.2.24.

596 11. Gouzy A, Larrouy-Maumus G, Wu T-D, Peixoto A, Levillain F, Lugo-Villarino G,
597 Guerquin-Kern J-L, de Carvalho LPS, Poquet Y, Neyrolles O. 2013. *Mycobacterium*
598 *tuberculosis* nitrogen assimilation and host colonization require aspartate. Nat Chem Biol
599 9:674–676.

600 12. Gouzy A, Poquet Y, Neyrolles O. 2014. Nitrogen metabolism in *Mycobacterium*
601 *tuberculosis* physiology and virulence. Nat Rev Microbiol 12:729–737.

602 13. Gouzy A, Larrouy-Maumus G, Bottai D, Levillain F, Dumas A, Wallach JB, Caire-Brandli
603 I, de Chastellier C, Wu T-D, Poincloux R, Brosch R, Guerquin-Kern J-L, Schnappinger D,
604 Sório de Carvalho LP, Poquet Y, Neyrolles O. 2014. *Mycobacterium tuberculosis* Exploits
605 Asparagine to Assimilate Nitrogen and Resist Acid Stress during Infection. PLoS Pathog
606 10:e1003928.

607 14. Smeulders MJ, Keer J, Speight RA, Williams HD. 1999. Adaptation of *Mycobacterium*
608 *smegmatis* to stationary phase. J Bacteriol 181:270-283.

609 15. Jack DL, Paulsen IT, Saier MH. 2000. The amino acid/polyamine/organocation (APC)
610 superfamily of transporters specific for amino acids, polyamines and organocations.
611 Microbiology 146:1797–1814.

612 16. Consortium TU, The UniProt Consortium. 2019. UniProt: a worldwide hub of protein
613 knowledge. Nucleic Acids Res 47:D506-D515.

614 17. Krogh A, Larsson B, von Heijne G, Sonnhammer EL. 2001. Predicting Transmembrane
615 Protein Topology with a Hidden Markov Model: Application to Complete Genomes. J Mol
616 Biol 305:567–580.

617 18. Edwards N, Anderson CHM, Conlon NJ, Watson AK, Hall RJ, Cheek TR, Embley TM,
618 Thwaites DT. 2018. Resculpting the binding pocket of APC superfamily LeuT-fold amino
619 acid transporters. Cell Mol Life Sci 75:921-938.

620 19. Owens DF, Kriegstein AR. 2002. Is there more to GABA than synaptic inhibition? Nat Rev
621 Neurosci 3:715–727.

622 20. Kim JK, Kim YS, Lee H-M, Jin HS, Neupane C, Kim S, Lee S-H, Min J-J, Sasai M, Jeong
623 J-H, Choe S-K, Kim J-M, Yamamoto M, Choy HE, Park JB, Jo E-K. 2018. GABAergic
624 signaling linked to autophagy enhances host protection against intracellular bacterial
625 infections. Nat Commun 9:4184.

626 21. Dagorn A, Hillion M, Chapalain A, Lesouhaitier O, Duclairoir Poc C, Vieillard J, Chevalier
627 S, Taupin L, Le Derf F, Feuilloley MGJ. 2013. Gamma-aminobutyric acid acts as a specific
628 virulence regulator in *Pseudomonas aeruginosa*. Microbiology 159:339–351.

629 22. Ferson AE, Wray LV, Fisher SH. 1996. Expression of the *Bacillus subtilis* gabP gene is
630 regulated independently in response to nitrogen and amino acid availability. Mol Microbiol
631 22:693-701.

632 23. McCraw SL, Park DH, Jones R, Bentley A, Rico A, Ratcliffe RG, Kruger NJ, Collmer A,
633 Preston GM. 2016. GABA (γ-Aminobutyic Acid) Uptake Via the GABA Permease GabP
634 Represses Virulence Gene Expression in *Pseudomonas syringae* pv. tomato DC3000. Mol.
635 Plant Microbe Interact. 29:938-949.

636 24. Dover S, Halpern YS. 1972. Utilization of γ-Aminobutyric Acid as the Sole Carbon and
637 Nitrogen Source by *Escherichia coli* K-12 Mutants. J Bacteriol 109:835-843.

638 25. Ma Z, Gong S, Richard H, Tucker DL, Conway T, Foster JW. 2003. GadE (YhiE) activates
639 glutamate decarboxylase-dependent acid resistance in *Escherichia coli* K-12. Mol
640 Microbiol 49:1309-1320.

641 26. Gong L, Ren C, Xu Y. (2020) GlnR Negatively Regulates Glutamate-Dependent Acid
642 Resistance in *Lactobacillus brevis*. Appl Environ Microbiol 86:e02615-19.

643 27. Seth A, Connel ND. 2000. Amino Acid Transport and Metabolism in Mycobacteria:
644 Cloning, Interruption, and Characterization of an L-Arginine/ γ-Aminobutyric Acid
645 Permease in *Mycobacterium bovis* BCG. J Bacteriol 182:919-927.

646 28. Alexandrov AI, Mileni M, Chien EYT, Hanson MA, Stevens RC. 2008. Microscale
647 Fluorescent Thermal Stability Assay for Membrane Proteins. Structure 16:351-359.

648 29. Rath A, Glibowicka M, Nadeau VG, Chen G, Deber CM. 2009. Detergent binding explains
649 anomalous SDS-PAGE migration of membrane proteins. Proc Natl Acad Sci U S A
650 106:1760–1765.

651 30. Hayashi Y, Matsui H, Takagi T. 1989. Membrane Protein Molecular Weight Determined
652 by Low-Angle Laser Light-Scattering Photometry Coupled with High-Performance Gel
653 Chromatography, Methods Enzymol 172:514-528.

654 31. Pressman BC, Fahim M. 1982. Pharmacology and toxicology of the monovalent carboxylic
655 ionophores. Annu Rev Pharmacol Toxicol 22:465–490.33.

656 32. Friesner RA, Banks JL, Murphy RB, Halgren TA, Klicic JJ, Mainz DT, Repasky MP, Knoll
657 EH, Shelley M, Perry JK, Shaw DE, Francis P, Shenkin PS. 2004. Glide: a new approach
658 for rapid, accurate docking and scoring. 1. Method and assessment of docking accuracy. J
659 Med Chem 47:1739-1749.

660 33. Gao X, Zhou L, Jiao X, Lu F, Yan C, Zeng X, Wang J, Shi Y. 2010. Mechanism of substrate
661 recognition and transport by an amino acid antiporter. Nature 463:828-832.

662 34. Warner DF. 2014. *Mycobacterium tuberculosis* Metabolism. Cold Spring Harb Perspect
663 Med 5:a021121.

664 35. Zaprasis A, Hoffmann T, Stannek L, Gunka K, Commichau FM, Bremer E. 2014. The γ-
665 aminobutyrate permease GabP serves as the third proline transporter of *Bacillus subtilis*. J
666 Bacteriol 196:515–526.

667 36. Kahane S, Levitz R, Halpern YS. 1978. Specificity and Regulation of γ-Aminobutyrate
668 Transport in *Escherichia coli.* J Bacteriol. 135:295-299.

669 37. Atkinson MR, Fisher SH. 1991. Identification of Genes and Gene Products Whose
670 Expression is Activated during Nitrogen-Limited Growth in *Bacillus subtilis.* J Bacteriol
671 173:23-27.

672 38. Bartsch K, von Johnn-Marteville A, Schulz A. 1990. Molecular Analysis of Two Genes of
673 the *Escherichia coli gab* Cluster: Nucleotide Sequence of the Glutamate:Succinic
674 Semialdehyde Transaminase Gene (*gab*T) and Characterization of the Succinic
675 Semialdehyde Dehydrogenase Gene (*gab*D). J Bacteriol 172:7035–7042.

676 39. Saidijam M, Bettaney KE, Szakonyi G, Psakis G, Shibayama K, Suzuki S, Clough JL,
677 Blessie V, Abu-Bakr A, Baumberg S, Meuller J, Hoyle CK, Palmer SL, Butaye P,
678 Walravens K, Patching SG, O'reilly J, Rutherford NG, Bill RM, Roper DI, Phillips-Jones
679 MK, Henderson PJF. 2005. Active membrane transport and receptor proteins from bacteria.
680 Biochem Soc Trans 33:867–872.

681 40. Zhao Z, Ding J-Y, Ma W-H, Zhou N-Y, Liu S-J. 2012. Identification and Characterization
682 of γ-Aminobutyric Acid Uptake System GabPCg (NCgl0464) in *Corynebacterium*
683 *glutamicum*. Appl Environ Microbiol 78:2596-2601.

684 41. Iversen LL, Kelly JS. 1975. Uptake and metabolism of γ-aminobutyric acid by neurones and
685 glial cells. Biochem Pharmacol 24:933-938.

686 42. Brechtel CE, King SC. 1998. 4-Aminobutyrate (GABA) transporters from the amine-
687 polyamine-choline superfamily: substrate specificity and ligand recognition profile of the
688 4-aminobutyrate permease from *Bacillus subtilis*. Biochem J 333:565–571.

689 43. Kellosalo J, Kajander T, Honkanen R, Goldman A. 2013. Crystallization and preliminary
690 X-ray analysis of membrane-bound pyrophosphatases. Mol Membr Biol 30:64-74.

691 44. Screpanti E, Padan E, Rimon A, Michel H, Hunte C. 2006. Crucial Steps in the Structure
692 Determination of the Na^+/H^+ Antiporter NhaA in its Native Conformation. J Mol Biol
693 36:192-202.

694 45. Moss FJ, Imoukhuede PI, Scott K, Hu J, Jankowsky JL, Quick MW, Lester HA. 2009.
695 GABA transporter function, oligomerization state, and anchoring: correlates with
696 subcellularly resolved FRET. J Gen Physiol 134:489–521.

697 46. Li X-D, Villa A, Gownley C, Kim MJ, Song J, Auer M, Wang D-N. 2001. Monomeric state
698 and ligand binding of recombinant GABA transporter from *Escherichia coli*. FEBS Lett
699 494:165-169.

700 47. Rehan S, Jaakola V-P. 2015. Expression, purification and functional characterization of
701 human equilibrative nucleoside transporter subtype-1 (hENT1) protein from *Sf9* insect cells.
702 Protein Expr Purif 114:99-107.

703 48. Corin K, Baaske P, Geissler S, Wienken CJ, Duhr S, Braun D, Zhang S. 2011. Structure and
704 function analyses of the purified GPCR human vomeronasal type 1 receptor 1. Sci Rep
705 1:172.

706 49. Parmar MM, Edwards K, Madden TD. 1999. Incorporation of bacterial membrane proteins
707 into liposomes: factors influencing protein reconstitution. Biochim Biophys Acta 1421:77–
708 90.

709 50. Pramod AB, Foster J, Carvelli L, Henry LK. 2013. SLC6 transporters: structure, function,
710 regulation, disease association and therapeutics. Mol Aspects Med 34:197–219.

711 51. Bae JH, Miller, KJ. 1992. Identification of Two Proline Transport Systems in
712 *Staphylococcus aureus* and Their Possible Roles in Osmoregulation. Appl Environ
713 Microbiol 58:471-475

714 52. Stark MJR. 1987. Multicopy expression vectors carrying the lac represser gene for regulated
715 high-level expression of genes in *Escherichia coli*. Gene 51:255–267.

716 53. Ma C, Hao Z, Huysmans G, Lesiuk A, Bullough P, Wang Y, Bartlam M, Phillips SE, Young
717 JD, Goldman A, Baldwin SA, Postis VLG. 2015. A Versatile Strategy for Production of
718 Membrane Proteins with Diverse Topologies: Application to Investigation of Bacterial
719 Homologues of Human Divalent Metal Ion and Nucleoside Transporters. PLoS One
720 10:e0143010.

721 54. Postis VGL, Rawlings AE, Lesiuk A, Baldwin SA. 2013. Use of *Escherichia coli* for the
722 production and purification of membrane proteins. Methods Mol Biol 998:33–54.

723 55. Smith PK, Krohn RI, Hermanson GT, Mallia AK, Gartner FH, Provenzano MD, Fujimoto
724 EK, Goeke NM, Olson BJ, Klenk DC. 1985. Measurement of Protein using Bicinchoninic
725 Acid. Anal Biochem 150:76-85.

726 56. Slotboom DJ, Duurkens RH, Olieman K, Erkens GB. 2008. Static light scattering to
727 characterize membrane proteins in detergent solution. Methods 46:73–82.

728 57. Agapova A, Serafini A, Petridis M, Hunt DM, Garza-Garcia A, Sohaskey CD, Luiz Pedro
729 Sório de Carvalho LP. 2019. Flexible nitrogen utilisation by the metabolic generalist
730 pathogen *Mycobacterium tuberculosis.* eLife 8:e41129.

731 58. Seigneuret M, Rigaud J-L. 1985. Use of the fluorescent pH probe pyranine to detect
732 heterogeneous directions of proton movement in bacteriorhodopsin reconstituted large
733 liposomes. FEBS Lett 188:101–106.

734 59. Huerta-Cepas J, Szklarczyk D, Heller D, Hernández-Plaza A, Forslund SK, Cook H, Mende
735 DR, Letunic I, Rattei T, Jensen LJ, von Mering C, Bork P. 2019. eggNOG 5.0: a hierarchical,
736 functionally and phylogenetically annotated orthology resource based on 5090 organisms
737 and 2502 viruses. Nucleic Acids Res 47:309-314.

738 60. Li W, Godzik A. 2006. Cd-hit: a fast program for clustering and comparing large sets of
739 protein or nucleotide sequences. Bioinformatics 22:1658-1659.

740 61. Katoh K, Misawa K, Kuma K, Miyata T. 2002. MAFFT: a novel method for rapid multiple
741 sequence alignment based on fast Fourier transform. Nucleic Acids Res 30:3059-3066.

742 62. Waterhouse AM, Procter JB, Martin DM, Clamp M, Barton GJ. 2009. Jalview Version 2--
743 a multiple sequence alignment editor and analysis workbench. Bioinformatics 25:1189-
744 1191.

745 63. Camacho C, Coulouris G, Avagyan V, Ma N, Papadopoulos J, Bealer K, Madden TL. 2009.
746 BLAST+: architecture and applications. BMC Bioinformatics 10:421.

747 64. Edgar RC. (2004) MUSCLE: multiple sequence alignment with high accuracy and high
748 throughput. Nucleic Acids Res 32:1792-1797.

749 65. Kalyaanamoorthy S, Minh BQ, Wong TKF, von Haeseler A, Jermiin LS. 2017.
750 ModelFinder: fast model selection for accurate phylogenetic estimates. Nat Methods
751 14:587-589.

752 66. Nguyen LT, Schmidt HA, von Haeseler A, Minh BQ. 2015. IQ-TREE: a fast and effective
753 stochastic algorithm for estimating maximum-likelihood phylogenies. Mol Biol Evol
754 32:268-274.

755 67. Huson DH, Scornavacca C. 2012. Dendroscope 3: an interactive tool for rooted phylogenetic
756 trees and networks. Syst Biol 61:1061-7.

757 68. Kim DE, Chivian D, Baker D. 2004. Protein structure prediction and analysis using the
758 Robetta server. Nucleic Acids Res 32:526-531.

759 69. Kelley L, Mezulis S, Yates CM, Wass MN, Sternberg MJE. 2015. The Phyre2 web portal
760 for protein modelling, prediction and analysis. Nat Protoc 10:845-858.

761

FIGURES

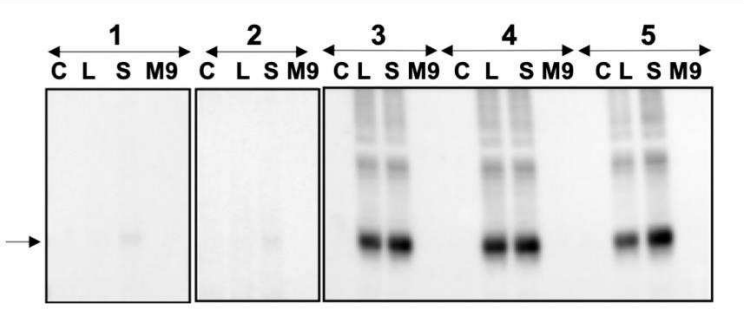

FIG 1 Expression of MsGabP. The expression of MsGabP in *E. coli* was analysed by western blotting (band migrating at ~36 kDa indicated by an arrow, detected by anti-HIS antibody). Lanes represent MsGabP expression results in: (1) C41 (DE3) Δ*acrB* pRARE2; (2) C43 (DE3) Δ*acrB* pRARE2 (3) C41 (DE3) Δ*acrB*; (4) BL21 Star (DE3) pRARE2; (5) BL21 Gold (DE3) pRARE2. Media type labelled as follows: C: LB media containing glucose; L: LB auto-induction media; S: SB auto-induction media; M9: M9 auto-induction media. The gels were spliced for labelling purposes.

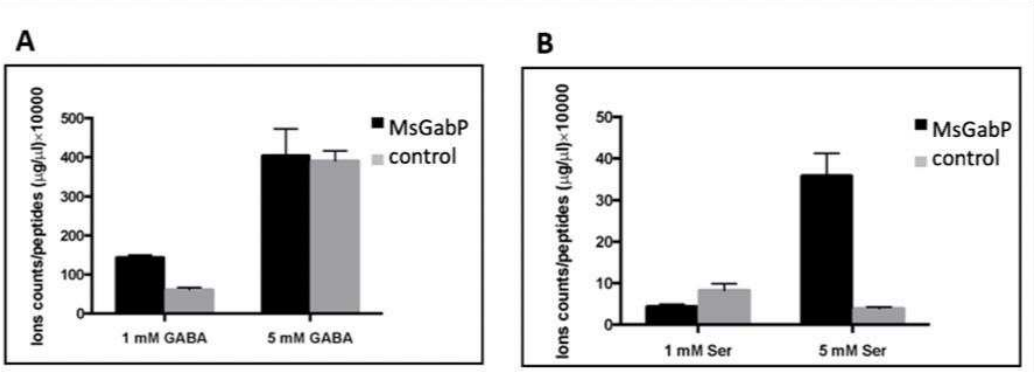

FIG 2 Targeted metabolomics study results of GABA (A) and serine (B). The amino acids were tested with two concentrations, 1 mM and 5 mM. The black and grey bar represents uptake resulted from cells harbouring plasmid with MsGabP or the empty vector as control, respectively. The charts show means (bars) and standard deviations (error bars) of three biological replicates of one independent experiment. They are representative of two independent experiments. They y-axes report the ion counts normalised on residual protein content (ions counts/peptides*1000).

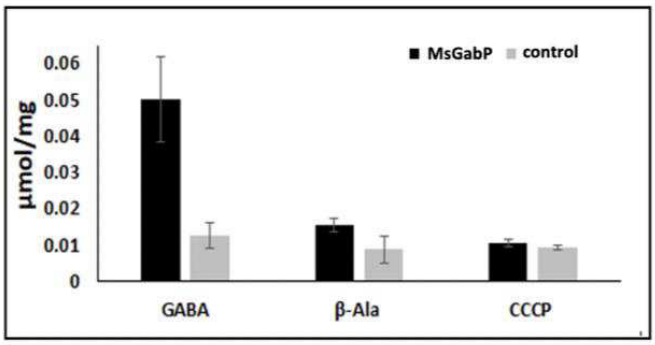

FIG 3 Direct measurement of [^{3}H]GABA uptake into *E. coli* cells. GABA: transport assay conducted in the presence of [^{3}H]GABA; β-ala: unlabelled 5 mM β-alanine was added before the addition of [^{3}H]GABA; CCCP: 50 µM CCCP was added before the addition of [^{3}H]GABA. The black and grey bar respectively represents the GABA uptake from cells harbouring plasmid with the GabP gene or empty vector. The data are means of three measurements. Error bars indicate standard deviations.

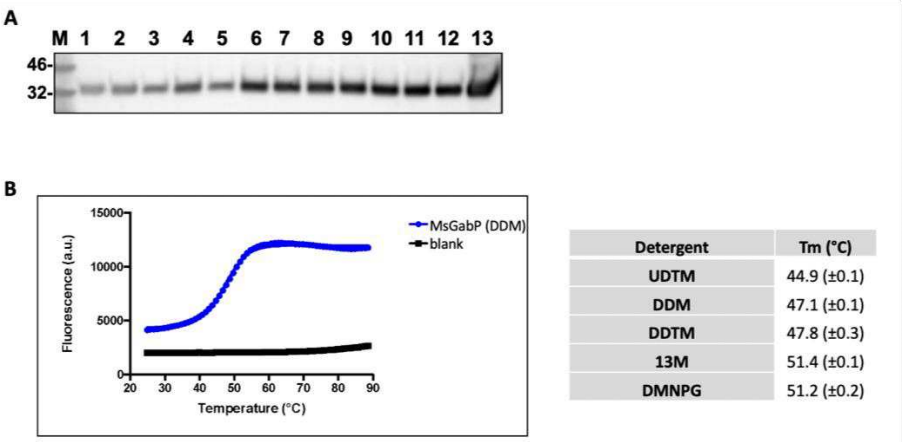

Detergent	Tm (°C)
UDTM	44.9 (±0.1)
DDM	47.1 (±0.1)
DDTM	47.8 (±0.3)
13M	51.4 (±0.1)
DMNPG	51.2 (±0.2)

FIG 4 Solubilisation of MsGabP. A) Detergent solubilisation screen. Anti-His Western blot of the supernatant fractions following solubilisation with: (1) CYMAL 6; (2) LMNPG; (3) DMNPG; (4) OGNPG; (5) β-OG; (6) 14M; (7) 13M; (8) DDTM; (9) DDM; (10) UDTM; (11) UDM; (12) DM; Lane 13 is a membrane fraction with no detergent added; M represent protein molecular marker (kDa). B) Microscale fluorescent thermal stability assay of MsGabP. GabP purified with DDM at pH 7.0. The blue line represents data points collected during the MsGabP unfolding process and the black line from buffer blank control samples. Table shows the summary of T_m values calculated from the melting curves. Values shown are means of two separate measurements.

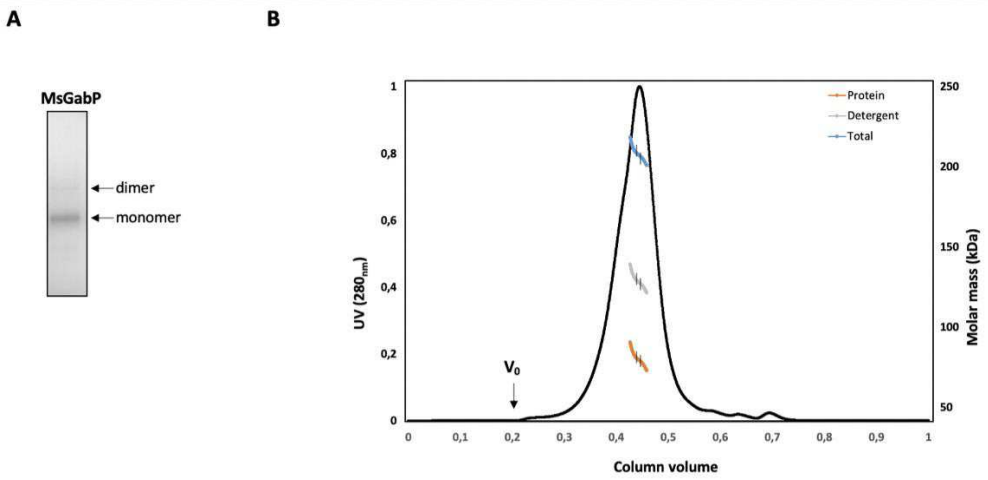

FIG 5 SEC-MALLS analysis of purified MsGabP. A) SDS-PAGE of MsGabP eluted in DMNPG. The arrows indicate the bands on the gel corresponding to MsGabP at ~36 kDa and ~70 kDa. B) SEC-MALLS UV chromatogram. The thick orange, grey and blue lines indicate the molar mass distribution of the eluting protein, detergent and total complex respectively (scale on the right-hand axis). Black lines indicate the part used for calculations of molar masses.

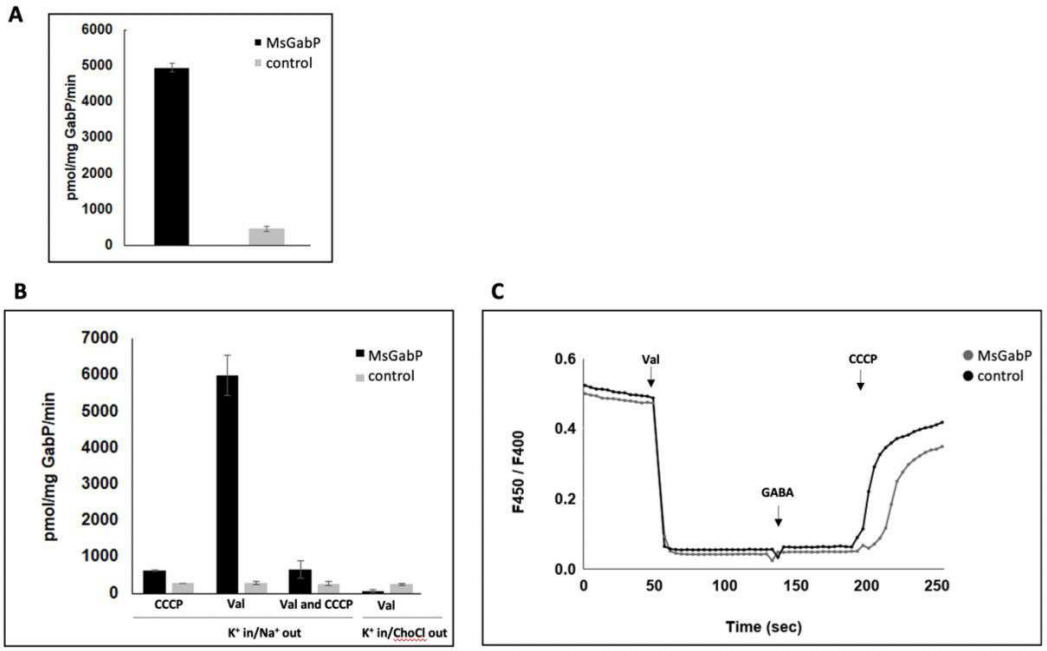

FIG 6 Transport activity of the purified MsGabP reconstituted into liposomes. Radioactive GABA uptake measured in the presence of 200 mM NaCl (A) and 200 mM NaCl or 200 mM choline chloride, in the presence and absence of valinomycin (5 nM) and/or CCCP (0.03 mM) (B). GABA transport was measured for 10 min. C) Monitoring of pH variation during GABA transport with pyranine. The ratio of fluorescence at 450:400 nm is shown over time. The black and grey bars represent uptake resulted from proteoliposomes containing MsGabP and protein-free liposome as control samples, respectively. All liposomes were loaded with 25 mM HEPES (pH 6.8), including 200 mM KCl. The data are means of three measurements. Error bars indicate standard deviations.

TABLES

Table 1. Detergents tested for solubilization efficiency and MsGabP yield after detergent exchange.

Detergent	Concentration (x CMC)	Concentration (%)	MsGabP yield after detergent exchange (%)
DDM	5.7	0.05	100
CYMAL 6	3	0.084	92.3
β-OG	3	1.59	0
OGNPG	3	0.174	35.9
DMNPG	3	0.0102	83.7
LMNPG	3	0.003	0
DM	3	0.261	71.8
UDM	5	0.145	84.8
UDTM	5	0.055	90.9
DDTM	5	0.013	51.5
13M	5	0.0085	72.7
14M	5	0.0027	0

n-Dodecyl-β-D-Maltopyranoside (DDM), 6-Cyclohexyl-1-hexyl-β-D-maltoside (CYMAL 6), n-Octyl-β-D-Glucopyranoside (β-OG), Octyl Glucose Neopentyl Glycol (OGNPG), Decyl Maltose Neopentyl Glycol (DMNPG), Lauryl Maltose Neopentyl Glycol (LMNPG), n-Decyl-β-D-Maltopyranoside (DM), n-Undecyl-β-D-Maltopyranoside (UDM), n-Undecyl-β-D-Thiomaltopyranoside (UDTM), n-Dodecyl-β-D-Thiomaltopyranoside (DDTM), n-Tridecyl-β-D-Maltopyranoside (13M) and n-Tetradecyl-β-D-Maltopyranoside (14M). Values in the column "MsGabP yield after detergent exchange (%)" shows protein yield after detergent exchange. The number was calculated using the amount of MsGabP obtained with eleven different detergents divided by the amount obtained from purification with DDM. CMC, critical micellar concentration.